KERNFORSCHUNGSZENTRUM

KARLSRUHE
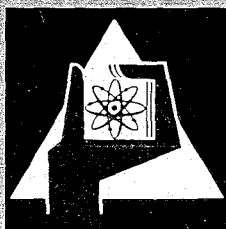
Juni 1967

Institut für Neutronenphysik und Reaktortechnik

Institut für Angewandte Kernphysik

Some Aspects of the Feasibility of a 10^{16}-Flux Reactor

M. Dalle Donne, J. Kallfelz, M. Küchle

KERNFORSCHUNGSZENTRUM KARLSRUHE

Juni 1967   KFK 579

Institut für Neutronenphysik und Reaktortechnik

Institut für Angewandte Kernphysik[++]

Some Aspects of the Feasibility of a 10^{16}-Flux Reactor

by

M. Dalle Donne[+], J. Kallfelz[++] and M. Küchle

[+] Delegated from EURATOM to the Fast Breeder Project, Institute of
     Neutron Physics and Reactor Engineering, Kernforschungszentrum Karlsruhe

[++] Now at the Georgia Institute of Technology, Atlanta, Georgia, U.S.A.

I. Introduction

With the operation of the HFBR, HFIR, and SM-2, and with the design of
the Franco-German and British high flux reactors, a new generation of
research reactors exists which produce fluxes in the $10^{15}/cm^2$ sec-range.
This is a considerable improvement over the conventional research reac-
tors with fluxes of about 10^{14}. This achievement was obtained by higher
performance, and now the development seems to be close to the limit of
present engineering techniques. However, at the International Seminar
on Intense Neutron Sources held in Santa Fe in September 1966, it was
pointed out that there is a continuous need for even higher neutron fluxes
to be used in nuclear and solid state physics applications. Though there
is a large class of experiments for which a steady state flux of $10^{15}/cm^2$ sec
is sufficient, and other experiments which can be made with a peak flux of
$10^{16}/cm^2$ sec obtained from a repetitively pulsed reactor, there are a number
of experiments which require a steady state flux of $10^{16}/cm^2$ sec or even
more [1,2,3]. A few examples are given below:

1. Studies of asymmetries in the ß-decay of polarized neutrons

   This is the best available measure of most of the fundamental parame-
   ters of the weak interaction and also furnishes an important test of
   time reversal invariance [1].

2. Studies of neutron-neutron interaction

   Since this interaction rate increases as the square of the flux whereas
   the background increases linearly with the flux, a higher flux than pre-
   sently available is required for an acceptable signal-to-background ratio.

3. In the field of neutron capture γ-rays, measurements of internal conver-
   sion spectra with a high resolution magnetic spectrograph and all meas-
   urements on materials with small capture cross sections.

4. In the field of fission physics, experiments where magnetic analysis is
   used to separate the fragments of a given mass.

5. For investigations of condensed matter, (a) single crystal diffrac-
   tion measurements where sample sizes are small. In particular, these
   are studies of organic crystals or biological molecules. (b) Measure-
   ments of the inelastic scattering of neutrons which cannot be well adapted
   to the conditions of a repetitively pulsed reactor.

Of course, these examples cannot illustrate completely the great improve-
ment which would be achieved with a 10^{16}-flux reactor. A large variety of
new experiments, for instance with very cold neutrons or with polarized
neutrons, would be possible and will be invented once the necessary high
flux is available. Moreover, all experiments could be improved in resolu-
tion, or in signal-to-background ratio, or in the time required for the
measurements.

Another important application is the production of transplutonium isotopes.
Since the production rate increases with a high power of the flux, the in-
centive to increase the flux is particularly high in this case.

In view of this interest in obtaining higher neutron fluxes, a preliminary
investigation was made in order to determine the engineering problems and
the economic implications of a 10^{16}-flux reactor. This reactor is also of
interest for comparison with a spallation type neutron source, such as the
Canadian project ING $\angle\overline{4}\,\overline{/}$.

A flux of $10^{16}/cm^2$sec can be obtained within present techniques with a
large dilute heavy water moderated reactor operating at about 1000 MW, as
the experience with the high flux charge at Savannah River indicates $\angle\overline{5}\,\overline{/}$;
possibly even higher flux at higher power may be attainable. However, a much
better ratio of flux to power and a better beam quality (ratio of thermal
to fast flux) can be obtained from a reactor with a small compact under-
moderated core surrounded by a D_2O-reflector which contains the beam tubes.

The purpose of this investigation was to study the possibilities and limi-
tations of such a concept, and a beam research reactor was taken as an example.
Some calculations were also made for an isotope reactor, and are given in the
Appendix. Since the work was stimulated by design calculations for the
Franco-German High Flux Reactor, some design features of this reactor were
maintained, such as the annular core with a one ring HFIR-type fuel element,
the beryllium plug in the center and the pressure barrel between core and
D_2O-reflector. The design parameters were pushed to the utmost limits and
some reasonable extrapolations beyond current engineering practices were
assumed. Only the basic features of the reactor were studied, and such
problems as safety, control, radiation damage, and engineering details were
not considered. For reasons of simplicity all calculations were made for a
reactor without beam tubes.

II. General

In this paragraph the materials and operating conditions chosen will be described, and the reasons for the particular choices will be given.

1. Coolant

As mentioned in Par. I, the reactor considered here has a very compact core. Thus, for the total power necessary to obtain a flux of $10^{16}/cm^2sec$, a very high power density is required. Three coolants, H_2O above the critical pressure, sodium, and H_2-gas, were considered for the thermodynamic calculations. These calculations were made to determine, for the same power density, which coolant gives the lowest maximum fuel clad temperature. The results showed that, for the conditions assumed, the higher maximum temperatures were for Na and H_2; hence supercritical H_2O was chosen as the coolant. Compared to H_2O, the following comments apply to the other two coolants:

i) H_2 – higher specific heat, but lower density;

ii) Sodium – higher heat transfer coefficient, but higher inlet temperature and lower specific heat.

Nuclear calculations were also made for a D_2O-cooled reactor. While the "rendement" [1] for this reactor was better than that of an H_2O-cooled reactor of the same dimensions, this advantage was overcome by a lower k_{eff} for the D_2O-reactor.

2. Coolant Conditions

At the high H_2O-velocities and small coolant channels necessary with the high power density, there is a pressure drop of about 50 Atm across the core. Hence an inlet pressure of 300 Atm was chosen to insure that the exit pressure is still supercritical. Supercritical pressure is necessary at the outlet of the core because the fuel wall temperature is far above the critical temperature of water.

The coolant velocity was limited by considerations of the mechanical integrity of the fuel plates (see Par. IV below).

---

[1] "rendement" = ratio of maximum flux in the external reflector to total power.

Considering corrosion problems, a lower velocity was also deemed desirable, although for these particular operating conditions it seems likely that the corrosion is not strongly velocity dependent (see Par. VII below). A velocity of 32 m/sec was chosen.

3. Cladding

Preliminary results showed that clad temperatures would be too high for aluminium. Inconel 625 was chosen as the cladding material, because of its good combination of superior high temperature creep properties, and resistance to corrosion (see Par. VII below).

4. Fuel

Stainless steel 16-13 [2] was chosen as the matrix material for the fuel element meat. A stainless steel matrix is appropriate for a high fuel loading, which is desired to increase the length of the operating cycle. The chosen material is softer than the Inconel cladding, which is an advantage for fabrication reasons.

The fuel is in the form of UO_2 (40 wt % of the meat), with uranium enrichment to 93% ^{235}U.

5. Overall Assembly and Dimensions

A thin core ring was necessary for several reasons. First, the fuel utilization is better for a thin core, since there is a smaller interior region of low flux. Secondly, the "critical velocity" of the radially-mounted fuel plates is greater for a lower plate width (see Par. IV below).

A central region of beryllium leads also to better fuel utilization, since there is a region of high flux at the core inner boundary also. A central region is at any rate necessary for fabrication reasons.

The height of the core is limited by several factors. The regions at the top and bottom of the core do not contribute as much as the central region to the maximum flux in the reflector. Also, the pressure drop and maximum clad temperature increase with height.

---

[2] Composition given in Par. III below.

The final overall dimensions chosen were as follows:

Inner Core Radius, R_i :   7.0 cm

Outer Core Radius, R_o :   13.5 cm

Core Height,   H :   100   cm

Core Volume,   V :   42   liters .

The fuel element dimensions were restricted to 0.5 mm "meat" and 0.15 mm
cladding by thermal stress considerations (see Par. VI below). The coolant
channel width was 1.2 mm; a smaller width would have caused an excessive
pressure drop.

6. Pressure Barrel

The pressure barrel, which was located between the core and the D_2O-reflec-
tor, was made of an aluminium alloy (Al Zn Mg Cu 0.5) of 1.4 cm thickness. The choice of this material
was based on reactivity considerations. Diffusion theory calculations (dis-
cussed in Par. III) showed that a 1 cm stainless steel barrel reduced k_{eff}
by about 20%. The aluminium barrel caused a reduction of only about 3.5 %
in k_{eff}.

Zircalloy was rejected because of excessive thermal stresses caused by the
γ-heating and its poor thermal conductivity.

With the aluminium alloy chosen, however, the temperature increase in the
barrel wall produced by the assumed γ-heating of 160 W/gr was only 60°C.
Thus, due to the very good mechanical properties of this alloy, the stres-
ses caused by temperature and water pressure were sufficiently below the
yield point.

III. Nuclear Calculations

1. Introduction

Most of the nuclear calculations were made with the Karlsruhe Nuclear Pro-
gram System NUSYS $\underline{/6/}$. This system contains various programs which allow
the generation of group cross sections and the calculation of reactor para-
meters with one- and two-dimension diffusion theory. The cross section
values used were the "ABN" data of ABAGJAN et al. $\underline{/7/}$, which is a 26-group
set. To investigate the problem of the thermal cross sections, which are
strongly spatially dependent in the core, several calculations were also
made with THERMOS $\underline{/8/}$, a thermalization transport theory program.

2. Material Regions and Cross Sections

The core composition was described in Par. II above. The supercritical H_2O-coolant had an average density of 0.97 g/cc. The approximate weight concentrations of the most important elements in Inconel 625 and stainless steel 16/13 [3] are given in Table 1 :

Table 1   Alloy compositions (wt %)

Material	Density at room temp.	Ref.	Cr	Ni	Fe	Mo	Nb
Inconel 625	8.44 g/cc	[9]	22.9	61.2		9.1	4.2
Stainless steel 16/13	8.0 g/cc	[10]	16.5	13.5	65.1		1.0

It was presumed that the UO_2-SS powder was compacted to 96% of its theoretical density, based on the data given in [11] for a similar case (SS 316, 35% UO_2). The density of the clad and meat have small corrections for their elevated temperatures. The values obtained for the compositions of the various mixtures are given in Table 2.

Table 2   Region mixtures

Mixture	Material	Density (atom/cc . 10^{-24})
1 (Trap)	Be	$1.22 \cdot 10^{-1}$
2 (Core - 100% Fuel)	Cr	$5.8 \cdot 10^{-3}$
	Fe	$8.8 \cdot 10^{-3}$
	H	$3.88 \cdot 10^{-2}$
	Mo	$8.7 \cdot 10^{-4}$
	Nb	$4.2 \cdot 10^{-4}$
	Ni	$9.6 \cdot 10^{-3}$
	O	$2.38 \cdot 10^{-2}$
	U^{235}	$1.74 \cdot 10^{-3}$
3 (Tank)	Al	$6.0 \cdot 10^{-2}$
4 (Reflector)	D	$6.64 \cdot 10^{-2}$
	O	$3.32 \cdot 10^{-2}$
5 (H_2O above core)	H	$6.50 \cdot 10^{-2}$
	O	$3.25 \cdot 10^{-2}$

[3] DIN 17 006 Nomenclature: X8 Cr Ni Mo V Nb 1613 .

The "100% Fuel" of mixture 2 refers to the mixture with the normal UO_2 concentration. For use for flux-flattening in the boundary regions, core mixtures with UO_2-concentrations of 70%, 50%, 35%, and 25% of that of mixture 2 were also calculated. The stainless steel 16/13 concentration in these mixtures was raised correspondingly.

3. Methods and Results of NUSYS Calculations

A two-dimensional calculation with the full 26-energy groups of the ABN-set would require a prohibitive amount of time. Hence a one-dimensional diffusion theory calculation was first made for an approximately equivalent spherical shell reactor. The "equivalent spherical shell"[4] had the same core thickness as for the final cylindrical two-dimensional calculation; the inner radius of the equivalent spherical shell core was determined by requiring that the central sphere has the same chord length as that of the cylindrical "trap" in the two-dimensional reactor. The spectra calculated for the equivalent sphere were then used to condense the group constants from 26 to 4 energy groups as follows:

ABN (26-Group) Set	Reduced (4-Group) Set	Energy
1 - 10	1	10.5 MeV - 21.5 keV
11 - 18	2	21.5 keV - 46.5 eV
19 - 25	3	46.5 eV - 0.215 eV
26	4	0.0252 eV

The thermal group constants for both sets are those of a room-temperature Maxwellian. These values were used, since the thermal spectrum is extremely spatially dependent, so that a condensation of the two or three lower ABN groups gives quite varied results for the core reduced set constants, depending on where in the core the condensing spectrum is taken from. Since the spectrum in the core middle is much "hotter" than this Maxwellian, these cross sections are quite rough. The effect of this fact is investigated in Par. III.4, below. Figures 1 and 2 show typical spectra for condensation in the core and reflector, respectively.

---

[4] The equivalence was in the sense that the calculated spectra should be appropriate for condensation. k_{eff} was quite different from that of the two-dimensional reactor.

Using the condensed cross sections, the final calculations were made using the two-dimensional diffusion theory code DIXY $\underline{/6/}$. These calculations were repeated for various configurations and combinations of boundary zones, with the following requirements:

1) core ring thickness $\lesssim$ 6.5 cm,
2) core height $\lesssim$ 100 cm,

until the following conditions were satisfied:

3) $k_{eff} \simeq 1.21$,
4) $F_{rad} \lesssim 1.7$,

where F_{rad} is the radial source density shape factor.

The reasons for desiring a limit on the core ring thickness and height, which led to 1) and 2), have been mentioned in Par. II.5.

Condition 3) was imposed to give sufficient excess reactivity for the following factors:

		Excess Reactivity
a)	Beam tubes	5%
b)	Xe and Sm	3%
c)	Stabile fission products	6.4%
d)	Uranium burnup	3%
e)	Control	1%
f)	Temperature	0.5%
	Total	18.9% .

The total of 18.9% excess reactivity corresponds to a value for k_{eff} of about 1.21. The figures are based on calculations for the Franco-German High Flux Reactor, FGHFR $\underline{/12/}$. a), c), e), and f) are about the same values as for the FGHFR. b) is lower than the value of 5% for the FGHFR, since for the reactor discussed here only about half the fissions are in the thermal group. d) is lower because of an average burn-up lower than for the FGHFR. All figures are estimated and somewhat high in order to be conservative.

For condition 4), the maximum value of F_{rad} was somewhat arbitrarily set at 1.7, to keep the power peaks at the core boundary within acceptable limits. This required that there be a number of core boundary regions with reduced fuel concentration.

Figure 3 shows the final configuration for the reactor, and the resulting dimensions and nuclear characteristics are contained in Table 5. The rendement has been corrected to the approximate value expected for $k_{eff} = 1.0$, based on calculations for the FGHFR. At the core-reflector interface there are four boundary zones, all 2.5 mm wide, with 25%, 35%, 50%, and 70% of the normal fuel concentration. At the "trap"-core interface one 2.5 mm zone with 70% fuel concentration was used.

Figure 4 shows the radial power distribution at the reactor midplane. Due to the fact that the thermal group constants used are for a Maxwellian, this distribution is very rough. However, as THERMOS calculations discussed in Par. III.4. below indicate, these peaks are probably overestimated, so that the results are conservative.

Based on the figures given in Table 5, a maximum thermal flux in the reflector of $10^{16}/cm^2$sec would be reached with a total power of 500 MW. This corresponds to an average power density of 11.9 MW/l, and a maximum power density of 25.6 MW/l.

4. Thermal Group Cross Sections

As mentioned above, the assumption of Maxwellian values for the fourth energy group is not accurate, since the thermal spectrum in the core becomes increasingly "hardened" as the distance from the boundary is increased. Thus the thermal cross sections become increasingly smaller as the interior of the core is approached.

To investigate the influence of this effect on k_{eff}, several diffusion theory calculations were made in which the thermal cross sections were reduced to half their original value. All of the thermal cross sections were changed, since all of the important cross sections have approximately a 1/v-dependence and would be equally changed by a spectral shift. Hence k_{eff} is relatively insensitive to this change; k_{eff} never changed more than 1% due to this variation. The change in the rendement was not more than 3%.

The most serious error caused by presuming constant Maxwellian cross section values is that the spatial distribution of the thermal fissions is not correctly calculated. The leveling of the fission distribution is an important problem in a reactor with a high uranium concentration. Therefore, the problem of the fission "peaks" was investigated using the program

THERMOS $/8/$, which calculates the spatially dependent thermal neutron spectrum using transport theory. Two one-dimensional slabs were calculated which corresponded to UO_2-concentrations of "100%" (Mixture 2, Table 2) and "25%". The slab consisted of a three cm "core" region, and a 15 cm reflector region. The hydrogen and deuterium scattering in the H_2O and D_2O was represented by Nelkin kernels, and the oxygen scattering was represented by a free gas with a mass of 16. All other core materials were grouped into one fictional material with the appropriate constant total scattering cross section. The core absorption cross section was that for the "100%" or "25%" UO_2-concentration, with a 1/v-dependence. At the two outer slab boundaries reflector boundary conditions were assumed, since these boundaries corresponded approximately to the middle of the core and maximum reflector thermal flux position in the NUSYS calculation. The results from a NUSYS calculation were used for the epithermal flux distribution, needed to calculate the source distribution in THERMOS. This flux distribution was practically constant.

Figure 5 shows how strongly the core thermal spectrum varies from the reflector interface to the middle of the core, for the 100% UO_2-concentration. Particularly for the core middle, presuming that the thermal group stops at 0.215 eV is very inaccurate. The average energy of the neutrons below 0.215 eV varies from 1.62 kT at a point in the reflector 15 cm from the core, to 3.47 kT in the core middle. Hence the energy dependent cross sections averaged over the spectrum up to 0.215 eV, i.e.

$$\int_0^{0.215\ eV} \emptyset\,(E,x)\ \sigma(E)\ dE \quad \Big/ \quad \int_0^{0.215\ eV} \emptyset\,(E,x)\ dE$$

are quite spatially dependent.

However, for our calculations what interests one is the spatial dependence of the thermal fissions, which describes the "peaks" in the power density. This dependence is the same as that of

$$\int_0^{0.215\ eV} \emptyset\,(E,x)\ \sigma_a(E)\ dE \quad \text{from THERMOS} ,$$

since the fission and absorption cross sections both have 1/v-dependence in the thermal energy range.

To compare with the THERMOS values, NUSYS calculations were made with the same geometry as for the THERMOS cases, but using the cross sections as for the NUSYS reactor calculations. Figures 6 and 7 compare the NUSYS and THERMOS results for the spatial dependence of the fissions caused by neutrons below 0.215 eV. As can be seen, in both cases the NUSYS calculations overestimate the thermal fission peaks. Thus it is probable that the fission peaks in the NUSYS reactor calculations are also overestimated, and these results are conservative. Also, since non-thermal fissions make a large contribution to the total fission distribution in the NUSYS calculations, the total fission peaks are not as much in error as are the thermal fission peaks.

IV. Cooling-Water Critical Velocity

The critical velocity is the velocity at which the modifications of local velocity resulting from a deflection of the plates produce across the plates a pressure difference sufficient to maintain the deflection.

To calculate the critical velocity it was assumed that the evolvent fuel element plates can be approximated by a circumference arc (see Figure 8). According to reference $/\overline{13}/$ the critical velocity of a flat plate with built-in edges with a width equal to the chord of the curved plate considered is given by:

$$v_c = \sqrt{\frac{15\, E\, a^3\, s_a}{\rho_a\, b^4 (1 - \nu^2)}} \tag{1}$$

where: E = Young's modulus of Inconel 625 at $508^{\circ}C = 1.785 \cdot 10^{12}$ dynes/cm^2

ν = Poisson's ratio of Inconel 625 at $508^{\circ}C = 0.319$ $/\overline{9}/$

a = plate thickness = 0.03 cm

b = chord of the curved plate = 8.8 cm

s_a = nominal thickness of flow channel = 0.12 cm

ρ_a = mean coolant density = 0.97 gr/cm^3 .

The resulting v_c is 5.61 m/sec. A considerable extrapolation of the graphs of reference $/\overline{13}/$ shows that a curved plate, with $\frac{b}{a} = 110$ and an arc of 1.42 rad., such as that considered in Figure 8, has a critical velocity about 18 times higher than the above value, i.e. about 100 m/sec.

This value was obtained with two simplifying assumptions:

a) The evolvent is approximated by a circumference arc. This is a pessi-
mistic assumption because the evolvent under an uniform pressure differ-
ence deforms in a way that the plate rotates about a point in the middle
which is not displaced /14/; thus the effective plate width is about half
of the real value.

b) The plate has been presumed homogeneous and formed by Inconel 625 at
$508^{\circ}C$, which is an optimistic assumption because the Young's modulus of
the meat is lower ($1.492 \cdot 10^{12}$ dynes/cm^2) than that of Inconel 625.

If the geometrical tolerances of the coolant channel and of the plates
were zero, one could theoretically work with a water velocity of 100 m/sec;
in practice, the small dimensional differences between adjacent channels
have a strong influence on the stresses on the fuel plates. To take into
account this effect, a rather high safety factor was assumed. The select-
ed velocity was 32 m/sec, which is equivalent to a safety factor of 3.

V. Heat Transfer Calculations

The pressure drop in the average channel is given by:

$$\Delta p(\text{Atm}) = 0.9869 \cdot 10^{-2} \cdot \rho_a v_a^2 \left[0.25 + \frac{\lambda_a H}{4 s_a} \right] \tag{2}$$

where

ρ_a = mean water density = 0.97 gr/cm^3

v_a = mean water velocity = 32 m/sec

0.25 gives the pressure loss and recovery at channel inlet and outlet

H = channel length = 100 cm

s_a = channel nominal thickness = 0.12 cm

λ_a = friction coefficient given by the Moody correlation /15/

= 0.0239, for a Reynolds number equal to $4.24 \cdot 10^5$ and a dimen-
sionless roughness of the wall equal to 0.002. To take into
account the temperature effect the physical properties of water
appearing in the Reynolds number have been evaluated at the
average fuel element wall temperature.

The resulting Δp is 51 Atm. This means a force acting on the core in
the vertical direction of about 14 tonnes.

The heat transfer calculation has been performed for the hot streak [5].
To take into account local variations of roughness the friction coeffi-
cient has been assumed to be 10% higher than the average. Due to geome-
trical tolerances it has also been assumed that the average thickness of
the cooling channel corresponding to the hot streak is 0.02 cm less than
the nominal value. The resulting water velocity at the hot streak is
therefore:

$$v \approx v_a \sqrt{\frac{\lambda_a}{\lambda} \cdot \frac{s}{s_a}} = 32 \sqrt{\frac{1}{1.1} \cdot \frac{0.1}{0.12}} = 27.8 \text{ m/sec} \tag{3}$$

In the core the fuel element surface is equal to 10^4 cm^2 per liter, so
that a maximum power density of 25.6 MW/l is equivalent to a maximum heat
flux of 2560 W/cm^2 = 612 cal/cm^{2}sec. For F_{ax} = 1.27 the average hot streak
heat flux is q_m = 482 cal/cm^{2}sec and the outlet water temperature is given
by:

$$T_3 = T_1 + \frac{2 q_m H}{c_{pm} \rho_m vs} = 40 + \frac{2 \cdot 482 \cdot 100}{1.288 \cdot 0.895 \cdot 2.78 \cdot 10^3 \cdot 0.1} = 342^\circ C \tag{4}$$

The hot streak water temperature in the middle of the core is:

$$T_2 = T_1 + \frac{q_m H}{c_{pml} \rho_m vs} = 40 + \frac{482 \cdot 100}{1.026 \cdot 0.895 \cdot 2.78 \cdot 10^3 \cdot 0.1} = 229^\circ C \tag{5}$$

These calculations must be performed by iteration because the specific heat
is rather strongly temperature dependent. The product ρv has been as-
sumed constant; in reality it varies like $\sqrt{\rho}$, because v^2 is constant,
but ρ varies little in the range of temperatures and pressures considered.

The fuel plate wall temperature has been calculated with the Colburn corre-
lation with an uncertainty factor equal to 0.85 /16/. The heat transfer
coefficients in the middle and at the outlet of the hot streak are respec-
tively:

[5] The hot streak is the line in the vertical direction at the point in
the radial direction where the axially integrated power has a maximum.

$$h_2 = 0.85 \cdot 0.023 \frac{k_2}{2s_a} \left(\frac{2 \rho_m v \, s}{\mu_2} \right)^{0.8} Pr_2^{0.33} =$$

$$= 0.85 \cdot 0.023 \frac{1.589 \cdot 10^{-3}}{2 \cdot 0.12} \left(\frac{2 \cdot 0.895 \cdot 2.78 \cdot 10^3 \cdot 0.1}{1.248 \cdot 10^{-3}} \right)^{0.8} 0.8435^{0.33}$$

$$= 3.70 \text{ cal/cm}^2 \text{sec}^\circ\text{C} \tag{6}$$

$$h_3 = 0.85 \cdot 0.023 \frac{1.167 \cdot 10^{-3}}{2 \cdot 0.12} \left(\frac{2 \cdot 0.895 \cdot 2.78 \cdot 10^3 \cdot 0.1}{0.785 \cdot 10^{-3}} \right)^{0.8} 1.043^{0.33}$$

$$= 4.22 \text{ cal/cm}^2 \text{sec}^\circ\text{C} \tag{7}$$

And the wall temperatures are given by:

$$T_{W2} = T_2 + \frac{q_{max}}{h_2} = 229 + \frac{612}{3.70} = 394^\circ\text{C} \tag{8}$$

$$T_{W3} = T_3 + \frac{q_3}{h_3} = 342 + \frac{344}{4.22} = 424^\circ\text{C} \tag{9}$$

The wall temperature varies very little in the second half of the core and it reaches a maximum of 424°C at the core outlet corresponding the hot streak.

These high temperatures require the use of supercritical water; the water must be sufficiently supercritical at the hot streak outlet to avoid a pseudo-burnout. The pressure of 249 Atm is considered sufficiently above the critical pressure (225 Atm).

The maximum temperatures inside the fuel plates are obviously in the middle of the core on the hot streak. The temperature at the interface cermet-Inconel is given by:

$$T_{I2} = T_{W2} + \frac{q_{max} s_2}{k_{Inc}} = 394 + \frac{612 \cdot 0.015}{0.0403} = 622^\circ\text{C} \tag{10}$$

where s_2 = thickness of the Inconel cladding

k_{Inc} = thermal conductivity of Inconel at 508°C .

The maximum cermet temperature is given by:

$$T_{C2} = T_{I2} + \frac{q_{max} s_1}{2 \cdot k_{cermet}} = 622 + \frac{612 \cdot 0.025}{2 \cdot 0.031} = 869 \ ^\circ\text{C} \ , \tag{11}$$

where

s_1 is equal to half the thickness of the cermet

the factor of 2 is given by the parabolic temperature distribution in the cermet

k_{cermet} is the cermet thermal conductivity.

In the previous calculation it has been assumed that no temperature difference exists at the interface between cermet and cladding.

VI. Thermal Stresses

The following assumptions were made:

a) The temperature distribution in a horizontal cross section of the fuel plates is symmetric with respect to the central plane; only strains in the axial direction have been considered.

b) The temperature distribution in the cermet is parabolic, while in the cladding it is linear.

c) The effect of the built-in edges is neglected.

Then the thermal stresses in the cermet and in the cladding are given respectively by:

$$\sigma_1(x) = \frac{K E_1}{1-\nu_1} - \frac{E_1}{1-\nu_1} \alpha_1 \left[\Delta T_c - (\Delta T_c - \Delta T_I) \frac{x^2}{s_1^2} \right] \qquad (12)$$

$$\sigma_2(x) = \frac{K E_2}{1-\nu_2} - \frac{E_2}{1-\nu_2} \alpha_2 \left[\Delta T_I - \frac{(\Delta T_I - \Delta T_W)(x - s_1)}{s_2} \right] \qquad (13)$$

where K is the strain in the axial direction, common to cermet and cladding, and is given by:

$$K = \frac{\dfrac{E_1 \alpha_1}{1-\nu_1} \dfrac{s_1}{3} (2 \Delta T_c + \Delta T_I) + \dfrac{E_2 \alpha_2}{1-\nu_2} \dfrac{\Delta T_I + \Delta T_W}{2} s_2}{\dfrac{E_1 s_1}{1-\nu_1} + \dfrac{E_2 s_2}{1-\nu_2}} \qquad (14)$$

The most dangerous thermal stresses are those corresponding to the maximum fuel plate temperatures, that is for:

ΔT_C = difference between maximum cermet temperature and room temperture = 869 - 20 = 849°C

ΔT_I = difference between maximum cermet-cladding interface temperature and room temperature = 622 - 20 = 602°C

ΔT_W = difference between fuel plate wall temperature at the middle of the hot streak and room temperature = 394 - 20 = 374°C .

The physical properties of cermet and Inconel involved are the following:

E_1 = Young's modulus of the cermet at 787°C =
$= 0.4\ E_{uo2} + 0.6\ E_{s.s.16/13} = 0.4 \cdot 17.45 \cdot 10^5 + 0.6 \cdot 13.7 \cdot 10^5$
$= 15.2 \cdot 10^5\ kg/cm^2$

α_1 = thermal expansion coefficient of cermet between 787°C and 20°C = thermal expansion coefficient of stainless steel 16/13 between 787°C and 20°C = 13.99 $\cdot 10^{-6}\ °C^{-1}$

ν_1 = Poisson's ratio of cermet at 787°C = $0.4\ \nu_{uo2} + 0.6\ \nu_{s.s.16/13}$
$= 0.4 \cdot 0.301 + 0.6 \cdot 0.33 = 0.3184$

E_2 = Young's modulus of Inconel at 508°C = $13.2 \cdot 10^5\ kg/cm^2$

α_2 = thermal expansion coefficient of Inconel between 508°C and 20°C
$= 14.0 \cdot 10^6\ °C^{-1}$

ν_2 = Poisson's ratio of Inconel at 508°C = 0.319 .

With these numerical values and s_1 = 0.025 cm, s_2 = 0.015 cm, equations (12,13) become:

$$\sigma_1(x) = 1.674 \cdot 10^7\ x^2 - 1.073 \cdot 10^4 \qquad (kg/cm^2) \qquad (15)$$

$$\sigma_2(x) = 0.770 \cdot 10^4 + 5.687 \cdot 10^5 (x-0.025) \quad (kg/cm^2) \qquad (16)$$

$\sigma_1(x)$ is always negative (compression) and has a maximum in the center of the cermet equal to -10,730 kg/cm^2. At the interface cermet-Inconel $\sigma_1(x)$ is equal to -270 kg/cm^2. $\sigma_2(x)$ is always positive (tension). At the interface cermet-Inconel $\sigma_2(x)$ = 7700 kg/cm^2, at the interface Inconel-water $\sigma_2(x)$ has a maximum equal to 16,230 kg/cm^2. The yield strength of Inconel 625 at the interface cermet-cladding (622°C) and cladding-water (394°C) are respectively 5090 kg/cm^2 and 5180 kg/cm^2. One can see then that the thermal stresses in Inconel, which should be the material giving strength to the plates, are very high. Thermal stresses about twice the yield strength are normally accepted, in our case, however, they are three times the yield strength.

Furthermore, the Inconel is subjected to the pressure of the cermet, which, being not able to sustain the axial compression caused by thermal stresses, tends to expand in the transversal direction. However, these transversal stresses in Inconel should be very small due to the very small rigidity of the cladding in the transversal direction.

Obviously, to reach definite conclusions, it would be necessary to confirm these calculations and assumptions by means of experiments. However, it appears that, in a first approximation, with these plates the factor limiting the temperatures, and, therefore, the heat fluxes is the thermal stress.

VII. Corrosion

As mentioned in Par. II, one of the reasons for choosing Inconel 625 for the cladding material is its great resistance to corrosion. The supercritical water used for the cooling in this investigation represents an extreme condition for the cladding material, and makes corrosion a very important problem. At cladding temperatures in the range needed for this reactor ($T_{max} \approx 530^{\circ}C$) the normal stainless steels are very suceptible to stress-corrosion cracking [17,18]. Nickel alloys and alloys of the Incoloy type show better resistance to corrosion in H_2O at high temperatures [19]. Two alloys in particular, Inconel 625 and Incoloy 800, have been tested rather extensively at General Electric to determine their corrosion characteristics in high-temperature H_2O [19-21]. For the test conditions, Inconel 625 showed corrosion resistance somewhat better than that of Incoloy 800 in the temperature range of interest here (about $530^{\circ}C$). Furthermore, Inconel 625 has a greater strength and better creep properties at high temperatures than Incoloy 800 [9,22].

Even with the data available for Inconel 625, the amount of corrosion of the fuel plates is extremely hard to estimate. Corrosion is a very complex phenomenon, and there are a number of parameters involved in a corrosion test, such as clad temperature, H_2O-velocity, H_2O-density, H_2O-temperture, and the heat transfer rate through the cladding. The tests made at General Electric [19-21] are for clad temperatures and velocities comparable to those of the reactor considered here, but for a much lower heat transfer rate and H_2O-density. Table 3 compares the conditions in the reactor considered here with those for one element of the G.E. test loop.

Table 3

	Element of GE test loop	Reactor considered here
H_2O-Pressure (Atm)	70	300 - 249
H_2O-Temperature (°C)	335 - 450	40 - 342
H_2O-Velocity (m/sec)	37 - 49	32
Clad Temperature (°C)	480 - 590	530 (max)
Heat Flux (w/cm^2)	55 (average)	2560 (max)
* Inconel 625 corrosion loss at 150 hours (mm)	$2.5 \cdot 10^{-4}$	

* Read from curve in /21/.

Since the corrosion is such a complex process, it is extremely difficult to extrapolate from the values obtained for the test loop conditions to determine those values which would be expected for the reactor conditions. However, LEISTIKOW /23/ has indicated that it would probably be a fair approximation to presume that, for the case considered here, the corrosion depends only on the clad surface temperature. This assumption is based on the fact that already in the conditions of the G.E. test loop, the oxide layer on Inconel 625 was extremely thin compared to that of most other metals, and was practically non-existent on much of the clad-surface. Hence, greater heat transfer and H_2O-density, which might in many cases contribute to a faster removal of oxide and associated faster corrosion, should not be expected to have a strong influence for the particular case under consideration here. If this assumption is correct, then one can see from Table 3 that the corrosion is negligible for the short cycle time of the reactor core (≈ 6 days, see Par. VIII).

Another factor which could influence corrosion is the effect of radiation with fast neutrons /19/, which was of course not present in the G.E. test loop. Unfortunately, there are no investigations of this effect known to us.

At any rate, the value for corrosion from Table 3, $2.5 \cdot 10^{-4}$ mm is about 600 times less than the clad thickness (0.15 mm). Hence, the corrosion could be many times greater than the value in Table 3, and still be within acceptable limits.

VIII. Core Lifetime

No burn-up calculations were made for this investigation. However, an estimate of the lifetime of the core was made using the following assumptions, and applying a correction based on burn-up calculations for the Franco-German High Flux Reactor:

a) The limiting point for burn-up is the point of maximum flux, on the core-reflector boundary.

b) During the core lifetime, the flux at the core-reflector boundary does not change.

c) For the uranium concentration at the boundary (≈ 170 g/l) the maximum allowable burn-up is 70%.

The following comment should be made concerning b). This assumption is, of course, not entirely correct, due to the change of the uranium spatial distribution during the period of operation. However, this assumption should give reasonable accuracy in the results, since at this point the thermal flux, which causes the major part of the burn-up at the boundary, comes primarily from "in-streaming" from the reflector. This in-streaming should not vary too much during the period of operation, for a constant maximum thermal flux in the reflector.

To calculate the allowable burn-up time the following expression was used:

$$U(t) = U(0) \, e^{- \sum_i \sigma_a^{\,i} \, \phi^i \, t} \tag{17}$$

where

$U(t) = {}^{235}U$-concentration at core-reflector interface

t = time after start of cycle

$\sigma_a^{\,i}$ = absorption cross section of i-th group of 4-group set

ϕ^i = flux in i-th group, at core-reflector interface .

Using assumption c), $U(t_m) / U(0) = 0.3$, one gets $\sum_i \sigma_a^i \phi^i t_m = 1.2$, where t_m is the time for maximum burn-up. Using the values from Table 4, one arrives at the result that $t_m = 5.6$ days.

Table 4   Core nuclear values at core outer radius (ϕ^i values based on maximum ϕ^{th} in reflector of $10^{16}/cm^2 sec$)

i	σ_a^i (barn)	ϕ^i ($cm^{-2} sec^{-1}$)
1	1.7	$1.1 \cdot 10^{16}$
2	14.5	$2.82 \cdot 10^{15}$
3	55.0	$2.1 \cdot 10^{15}$
4	603.	$3.3 \cdot 10^{15}$

This calculation was checked by using the same method to calculate the cycle time for two cases considered for the Franco-German High Flux Reactor and comparing the results with those of accurate burn-up calculations which existed for the same cases. The accurate burn-up calculations were performed using the two-dimensional diffusion code TURBO $\underline{/24/}$. For both cases the results using expression (17) were about 4.5% lower than those from the TURBO calculations. Hence the corrected core lifetime for the case considered here is about $(1.045)(5.6) \approx 6$ days.

IX.   Fuel Cycle Costs

For the fuel elements envisaged - i.e. UO_2 in stainless steel matrix with Inconel clad - no statements on the reprocessing and refabrication costs can presently be made. But in order to get at least a rough idea of the annual fuel cycle costs of the reactor, two cases were considered:

a)   Optimistic - The fabrication and reprocessing costs are presumed to be the same as those for a core with aluminium as the "meat" matrix and fuel plate cladding ("aluminium core").

b)   More realistic - The fabrication costs are 3 times, and the reprocessing costs are 1.5 times those of an aluminium core.

The yearly fuel cost "K" is related to the cost per core, K_{core}, through:

$$K = \frac{365}{T+2} \cdot K_{core} \tag{18}$$

where T = cycle time for one core in days.

Two days are allowed for changing the core. With T = 6 (see Par. VIII), $K \approx 45\ K_{core}$.

Because of large uncertainties in the cost approximation, a greatly sim-plified equation can be used to calculate K_{core}:

$$K_{core} = K_{fabr} + K_{repr} + \beta K_u \tag{19}$$

where K_{fabr} = fabrication costs

K_{repr} = reprocessing costs

K_u = uranium cost for a core

β = average burn-up = 0.12 .

The core being considered contains 25 kg of ^{235}U. With a uranium price of 43.2 DM/g [25], βK_u = 0.13 $\cdot$ 10^6 DM.

Case a)

The reprocessing costs are about $(1-\beta) \cdot 1600$ DM/kg for an aluminium core [26]

Then K_{repr} = 0.40 $\cdot$ 10^6 DM ,

furthermore K_{fabr} = 0.30 $\cdot$ 10^6 DM .

Thus K_{core} = 0.83 $\cdot$ 10^6 DM ,

and   K   = 37 $\cdot$ 10^6 DM/yr .

Case b)

For this case: K_{repr} = 0.606 $\cdot$ 10^6 DM ,

and K_{fabr} = 0.900 $\cdot$ 10^6 DM .

Then K_{core} = 1.63 $\cdot$ 10^6 DM .

Thus the cost for the uranium used is less than 10% of the total fuel cycle cost. The yearly fuel cost is K = 73 $\cdot$ 10^6 DM/yr.

Use of a more accurate formula which also takes into account the fuel interest rates and the dependence of the reprocessing costs on the enrichment would increase both total costs by about 10%.

X. Conclusions

A summary of the important characteristics of the reactor is given in Table 5. One can see that it is possible to obtain a maximum thermal flux in the reflector of $10^{16}/cm^2$sec with a total power of 500 MW.

However, this relatively low total power implies a very high power density, which in turn leads to high fuel element temperatures. Therefore, Inconel 625 was chosen as the cladding material. Due to the low thermal conductivity of this alloy, the limiting factor for the power density is the magnitude of the thermal stresses. The thermal conductivity of aluminium is much higher. However, even if we assume that the geometrical tolerances of the fuel plates are zero, the maximum temperature in the aluminium plates is too high (about $370^{\circ}C$) to permit the use of this metal.

On the other hand, if one wants a neutron flux in the reflector of $0.5 \cdot 10^{16}$ n/cm^2sec only, then this is probably possible with aluminium (maximum hot spot temperature estimated at less then $300^{\circ}C$). The fuel cycle costs would be about four times smaller, due to smaller fabrication costs. It is evident that the step from $0.5 \cdot 10^{16}$ n/cm^2sec to $1 \cdot 10^{16}$ n/cm^2sec, which requires the use of Inconel 625 in place of aluminium as cladding material, is achieved with a considerable decrease (2 times) in the ratio neutron flux to fuel cycle costs.

The very short operating cycle and the large fraction of costs which goes into core fabrication leads one to consider other types of reactors, such as a homogeneous reactor. However, in our opinion the technical problems associated with homogeneous reactors are even more complicated than the type we considered in this report. Due to the extremely high costs and experimental inconvenience associated with such a short cycle, more detailed investigations were not made. Many further problems were not considered, such as:

1) radiation damage and sealing of the pressure barrel,
2) radiation damage and heat dissipation in the beam tubes,
3) thermal stresses in the fuel plates due to temperature gradients in the radial direction
4) heat removal from a cold source,
5) support of a core with an inlet-outlet pressure difference of 50 Atm.

Table 5   Preliminary design characteristics of a 10^{16}-flux beam research reactor

1. Dimensions and composition			2. Operating characteristics	
D₂O-reflector:	diameter	300 cm	Coolant velocity	32 m/sec
	height	200 cm	Coolant temperature at core entry	40° C
	pressure	near atmospheric	Mean coolant temperature at core exit	160° C
H₂O-core:	diameter	27 cm	Maximum coolant temperature at core exit	342° C
	height	100 cm	Pressure at core entry	300 Atm.
	central flux trap filled with Be, diameter	14 cm	Pressure at core exit	250 Atm.
	core volums	42 l	Maximum heat flux	2560 W/cm²
Al-pressure barrel:	between core and refelctor,		Average heat flux	1190 W/cm²
	thickness	1.4 cm	Maximum wall temperature of fuel plate	530° C
Fuel element:	one ring HFIR-type with radial power flattening		Maximum power density	25.6 MW/l
			Average power density	11.9 MW/l
meat:	stainless steel 16/13 with 40 % fully enriched UO₂	0.5 mm	Total power	500 MW
			Maximum unperturbed flux in the reflector	$1.0 \cdot 10^{16}$ /cm² sec
clad:	INCONEL 625	0.15 mm	k_{eff} of fresh core	1.21
	coolant channel width	1.2 mm	Length of cycle	6 d
	average fuel load	680 235U/l	Average burn-up	12 %
Coolant:	supercritical water			

Appendix A :   Isotope Reactor

An "isotope reactor", i.e., one which has the maximum flux in the cen-
tral trap, was also calculated. The core composition and the overall
dimensions were the same as for the beam reactor (except that the outer
radius of the reflector was only 45 cm for this case).

For the isotope reactor, the central trap was filled with H_2O, and the
reflector was Be. There was no pressure barrel for this case. Further-
more, the core boundary zones were switched so that there were 2.5 mm
zones of 25%, 35%, 50%, and 70% fuel concentration on the inner core
boundary, and 50% and 70% on the outer boundary. The factors such as
$F_{ax} \cdot F_{rad}$, k_{eff}, etc. were practically the same as for the beam reactor.
The thermodynamic characteristics were presumed to be essentially the
same as those of the beam reactor. For the same total power as the
beam reactor, i.e., 500 MW, the maximum thermal flux in the trap center
was about $2 \cdot 10^{16}$. No calculations were made for the case of a loaded
trap.

References

/1/ BOLLINGER, L.M., Nuclear Physics Experiments Performed with Neutrons, Proc. of the AEC-ENEA Seminar on Intense Neutron Sources, Santa Fe (1966)

/2/ BRUGGER, R.M., Studies of Condensed Matter Using Neutrons; Proc. of the AEC-ENEA Seminar on Intense Neutron Sources, Santa Fe (1966)

/3/ HARVEY, J.H., Neutron Cross Sections and Related Measurements, Proc. of the AEC-ENEA Seminar on Intense Neutron Sources, Santa Fe (1966)

/4/ Atomic Energy of Canada Ltd., The AECL Study for an Intense Neutron-Generator, AECL-2600 (1966)

/5/ CRANDALL, J.L., The Savannah River High Flux Demonstration, DP 999 (1965)

/6/ BACHMANN et al., NUSYS II, Internal Report INR-216/66, Kernforschungszentrum Karlsruhe (1966)

/7/ ABAGJAN et al., Gruppenkonstanten schneller und intermediärer Neutronen für die Berechnung von Kernreaktoren, KFK-tr-144, Kernforschungszentrum Karlsruhe

/8/ HONECK, H.C., THERMOS, A Thermalization Transport Theory Code for Reactor Lattice Calculations, BNL-5826, Brookhaven National Lab. (1961)

/9/ Preliminary Data INCONEL alloy 625, Huntington Alloy Products Division, The International Nickel Company, Inc., Huntington 17, West Virginia

/10/ Werkstoffe, Werkstoff-Blatt 550, Mannesmann AG., Düsseldorf Januar (1965)

/11/ KELLER, D.L., in Reactor Handbook, 2nd Ed. C.P. Tipton, Ed., Vol.I, Materials, p.316, Interscience Publishers, Inc., New York (1960)

/12/ BECKURTS, K.H., DAUTRAY, R., Project Studies for the Franco-German High Flux Reactor, Proc. of the AEC-ENEA Seminar on Intense Neutron Sources, Santa Fe (1966)

/13/ MILLER, D.R., Critical Flow Velocities for Collapse of Reactor Parallel-Plate Fuel Assemblies, KAPL-1954, Knolls Atomic Power Laboratory (1958)

/14/ The High-Flux Isotope Reactor, p.7-14, ORNL-3572, Oak Ridge National Laboratory (1965)

/15/ MOODY, L.F., Friction Factors for Pipe Flow, Trans.Am.Soc. Mech. Eng. 66, 671 (1944)

/16/ DALLE DONNE, M. and S. FABREGA, The French-German High Flux
      Reactor Core Thermal Study, to be printed

/17/ DRALEY, J.E., et al., Corrosion in Aqueous Systems, A/Conf.28/
      P/243, Third U.N. Int. Conf. PUAE, Geneva (1964)

/18/ ZINN, W.H. and J.R. DIETRICH, Ed. Power Reactor Technology, Vol.6,
      No.1, p.50, USAEC (1962)

/19/ BÖHM, H. and H.U. BORGSTEDT, Zur Frage der Hüllmaterialauswahl
      für einen dampfgekühlten Schnellen Brüter, Internal Report
      IMF-Nr. 20/66, Kernforschungszentrum Karlsruhe (1966)

/20/ PEARL, W.L., et al., Nuclear Applications, Vol.1, p.235, June (1965)

/21/ LEISTIKOW, S., Internal Report NSPE-Reisebericht Nr. 9/SL, Kern-
      forschungszentrum Karlsruhe (1965)

/22/ Engineering Properties of Incoloy 800, Tech.-Bulletin T-40,
      Huntington Alloy Products Division, The International Nickel Com-
      pany, Inc. (1961)

/23/ LEISTIKOW,S., private communication (1966)

/24/ GELBHARD,E., et al., TURBO, A Two Dimensional Few-Group Depletion
      Code for the IBM 704, WAPD-TM-95

/25/ ESCHNAUER,H., Atomwirtschaft VII, Heft 7, 8 (1962)

/26/ SCHARMER,K., private communication.
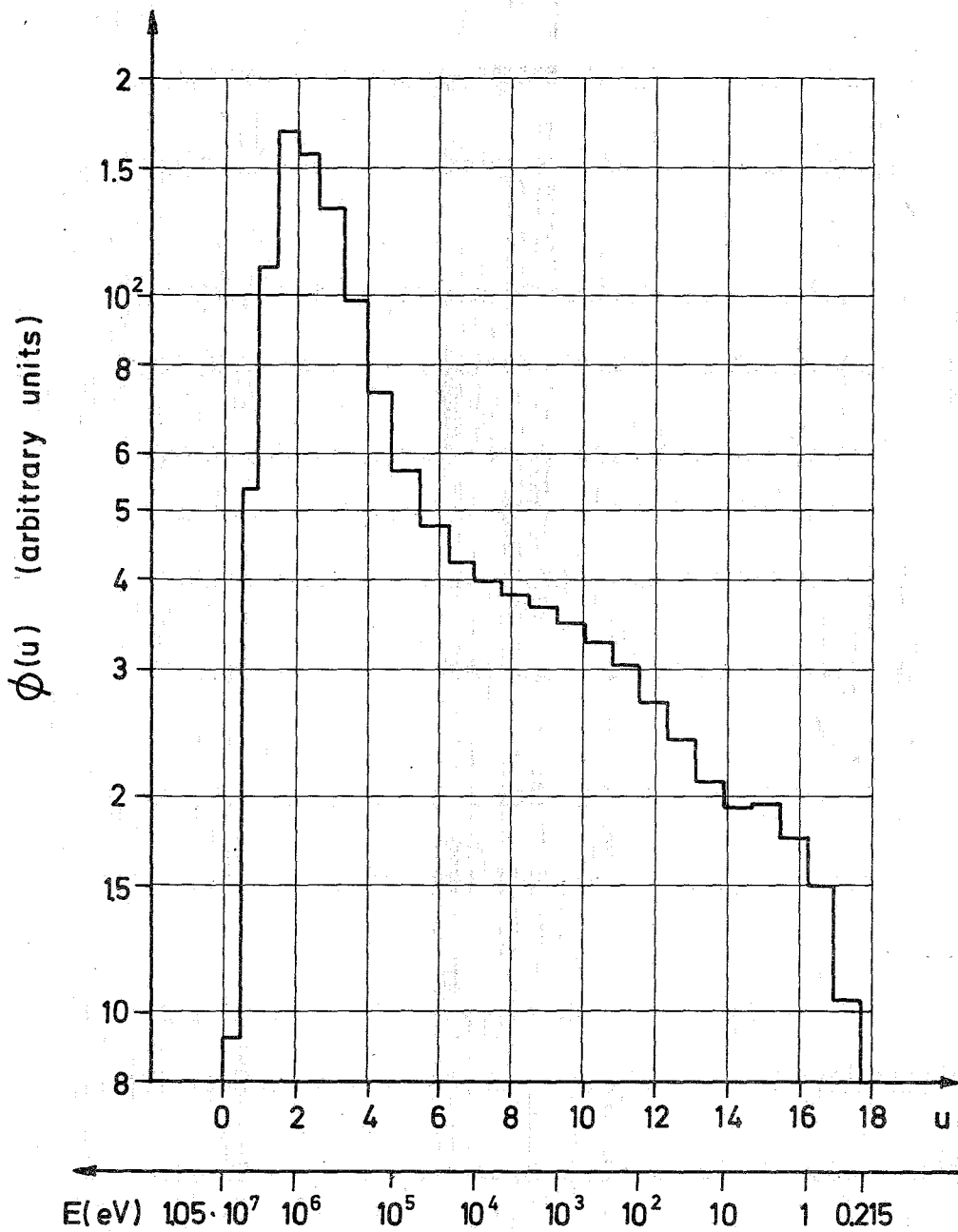
Fig.1. Spectrum from 26-group diffusion theory calculation used for condensation of group constants of mixture 2, Table 2 (core-100% fuel) from 26- to 4-groups (see Par. III.3.).
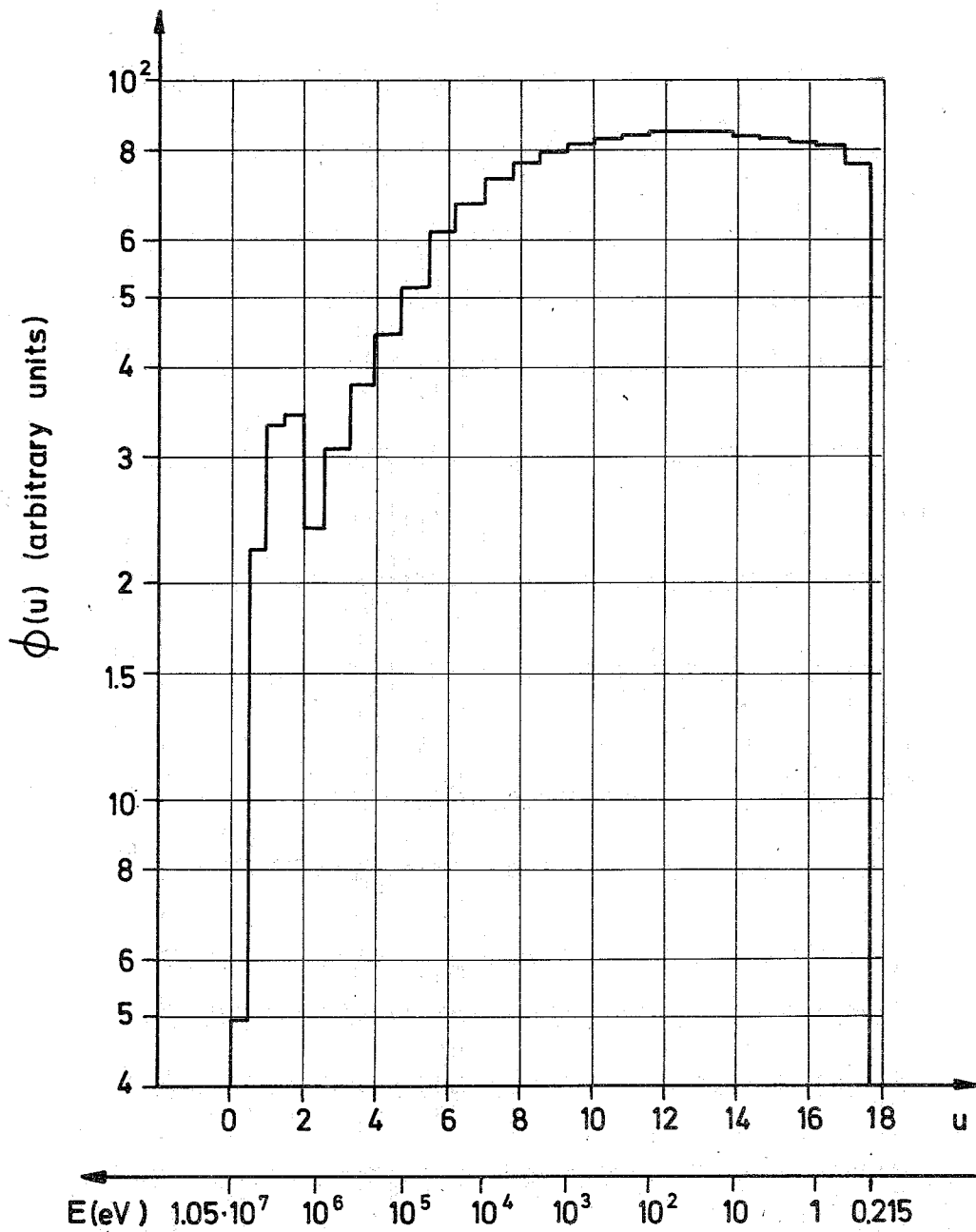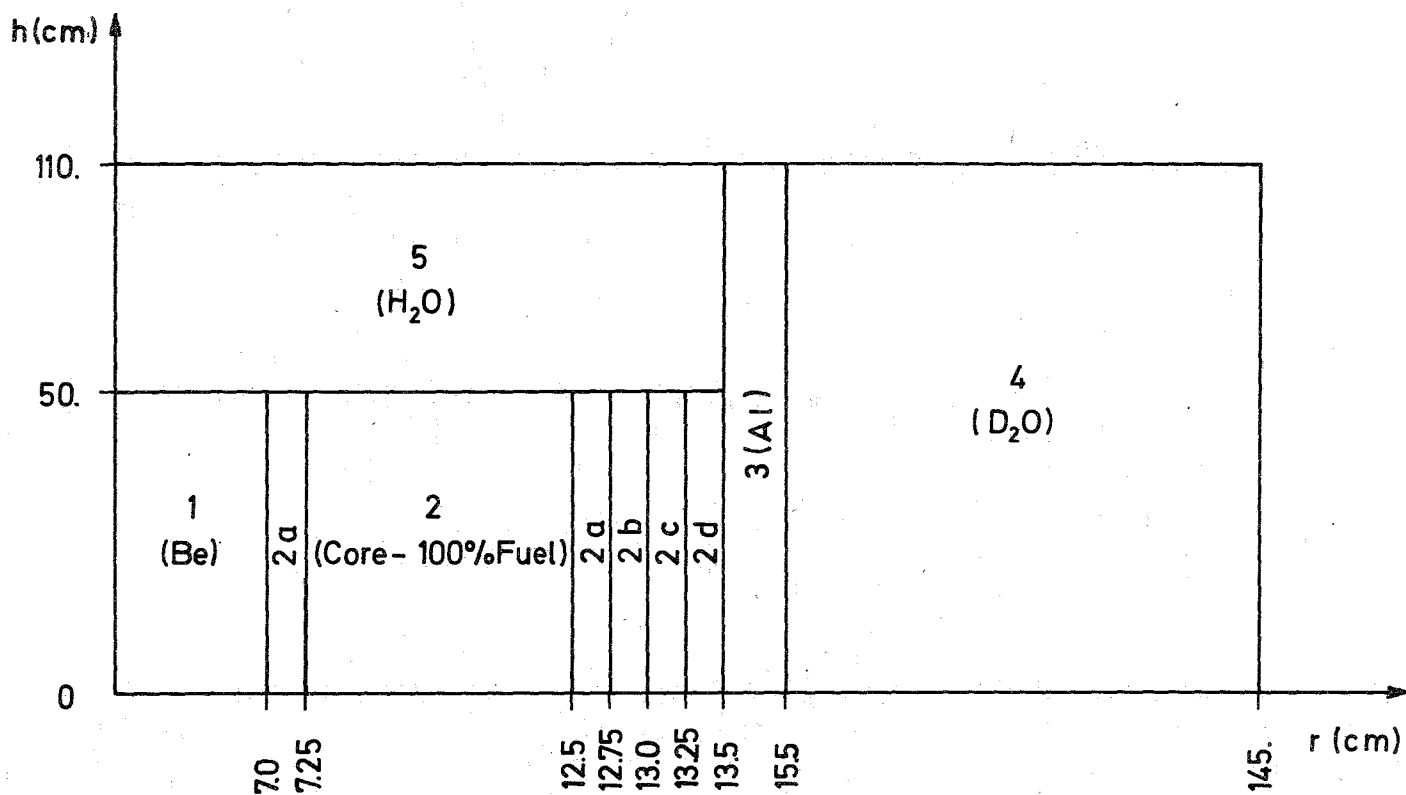
Lethargy, $u = \ln(E^*/E)$ where $E^* = 10.5$ MeV.

Fig.2.   Spectrum from 26-group diffusion theory calculation used for condensation of group constants of mixture 4, Table 2 (D_2O-reflector) from 26- to 4-groups (see Par. III.3.).

Lethargy, $u = \ln (E^*/E)$ where $E^* = 10.5$ MeV.

Fig.3. Quarter cross-section of configuration for final beam reactor calculation. The numbers are those of the mixtures in Table 2. 2a, 2b, 2c, and 2d are the core mixtures with UO_2-concentrations of 70%, 50%, 35%, and 25% of that of mixture 2, respectively.
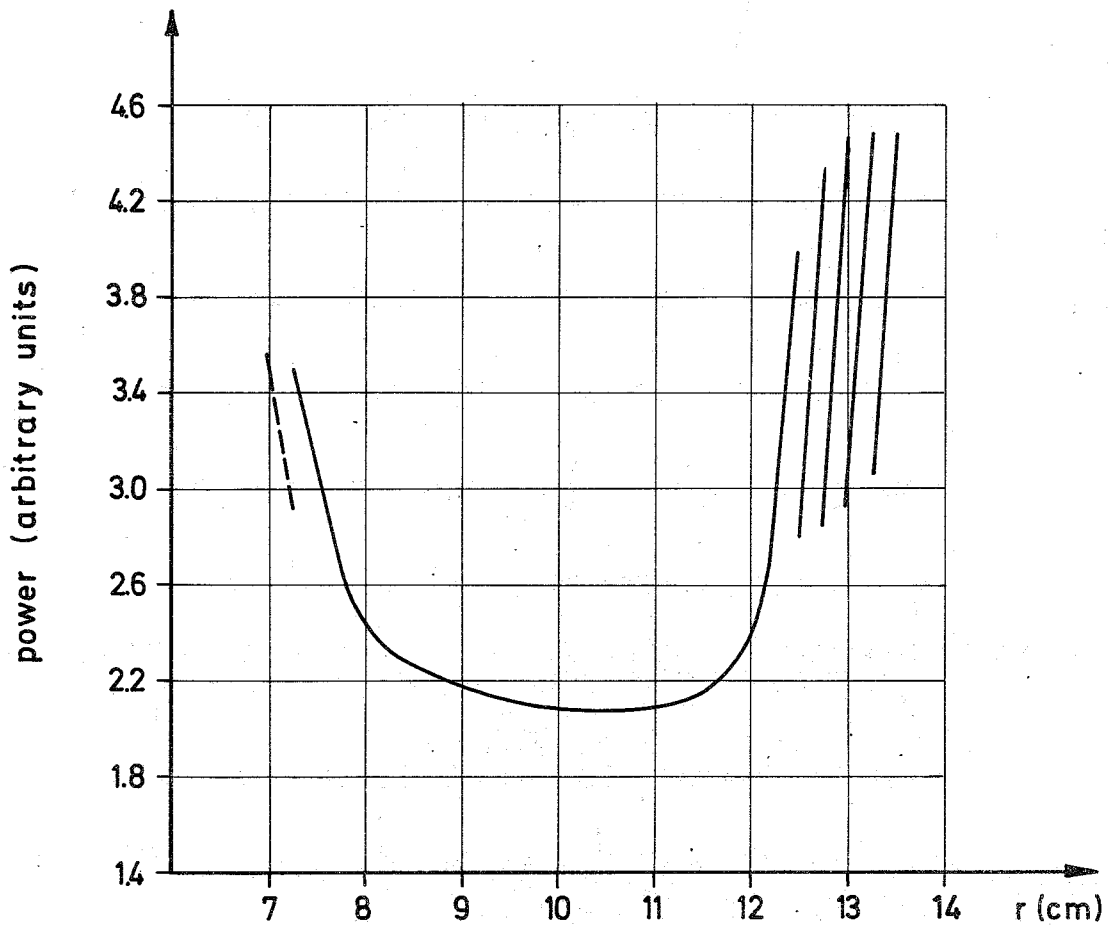
Fig.4. Radial power distribution at beam reactor midplane, for final 4-group diffusion theory calculation.

(— — — —)Only one point, at $r = 7$ cm, calculated in this region. At boundary points between various core zones, power values were not calculated; curves were extrapolated graphically to these points.
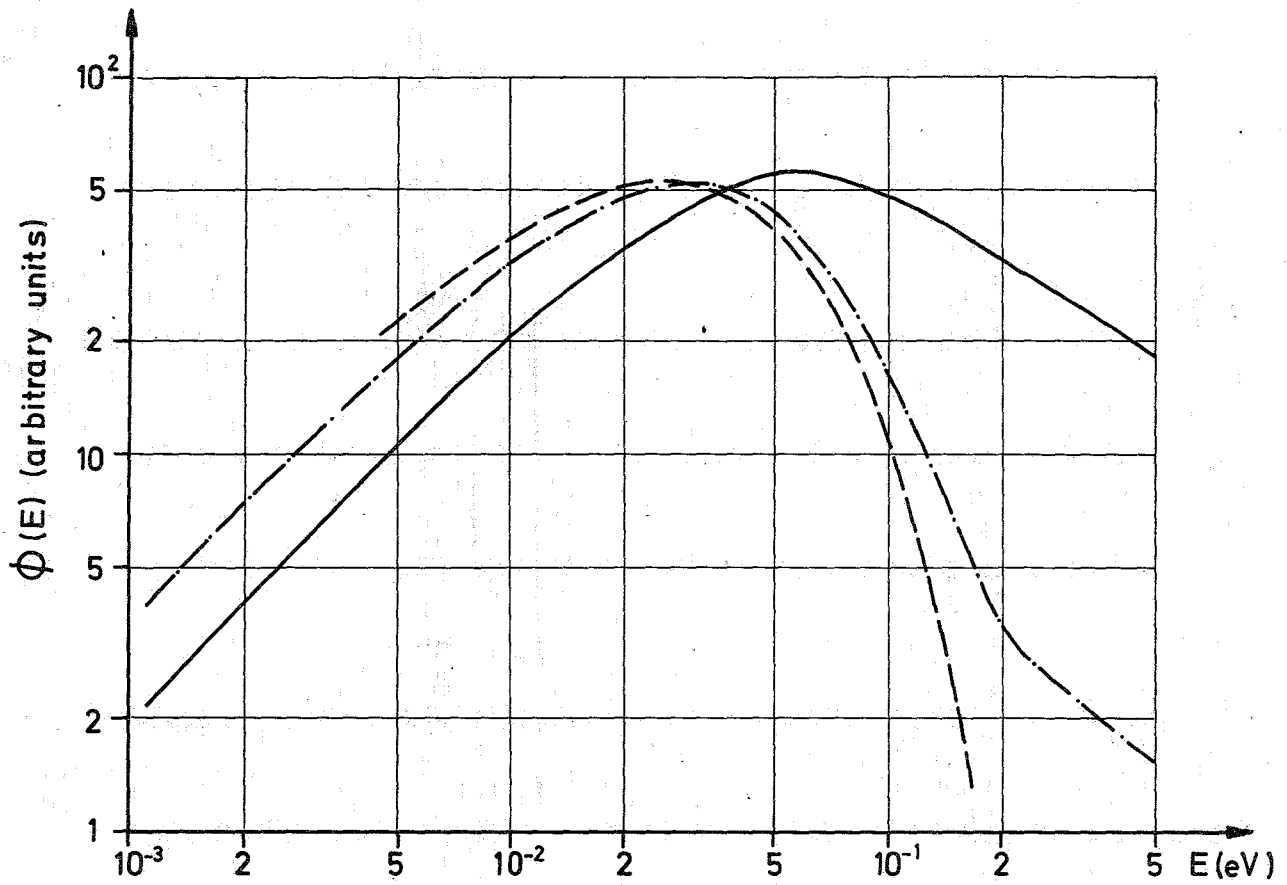
Fig.5. Results for core thermal spectra from THERMOS (see Par. III.4.).

———— 3 cm from core-reflector interface (approximately middle of core)

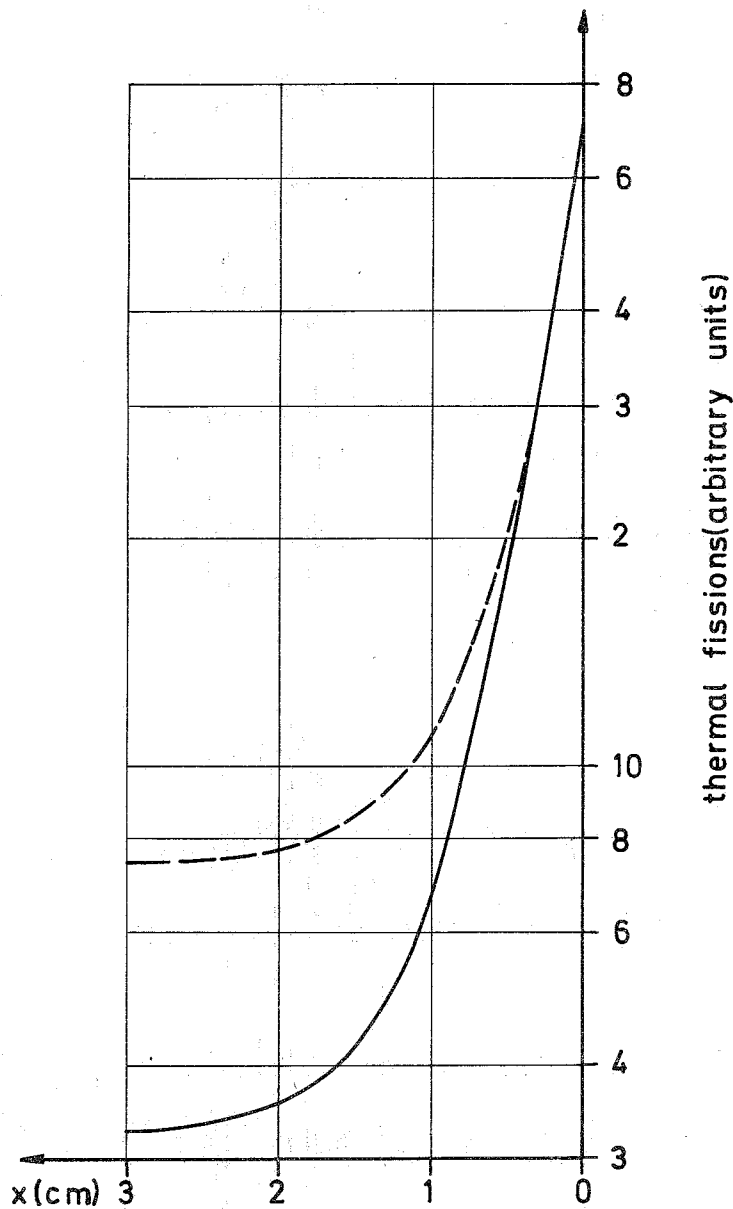—·—·— In core at core-reflector interface

—————— Maxwellian distribution

Fig.6.   Thermal fission distribution as function of distance, x, from core-reflector interface, for UO$_2$-concentration that of mixture 2, Table 2 (see Par. III.4.).

———————— 4-group diffusion theory calculation; $\emptyset \, \sigma_f$ of 4th (thermal) group

— — — — — THERMØS calculation; $\displaystyle\int_0^{0.215 \text{ eV}} \sigma_a(E) \, \emptyset(x,E) \, dE$
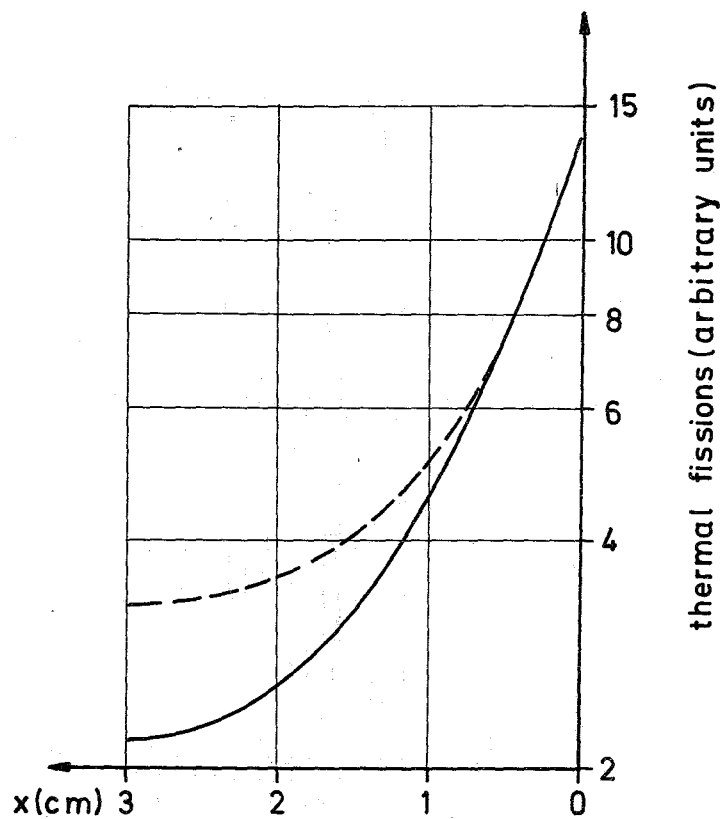
Fig.7. Thermal fission distribution as function of distance, x, from
core-reflector interface, for UO_2-concentration 25% that of
mixture 2, Table 2 (see Par. III.4.).

————————— 4-group diffusion theory calculation;
$\emptyset\ \sigma_f$ of 4th (thermal) group

— — — — — THERMØS calculation; $\displaystyle\int_{0}^{0.215\ eV} \sigma_a(E)\ \emptyset(x,E)\ dE$
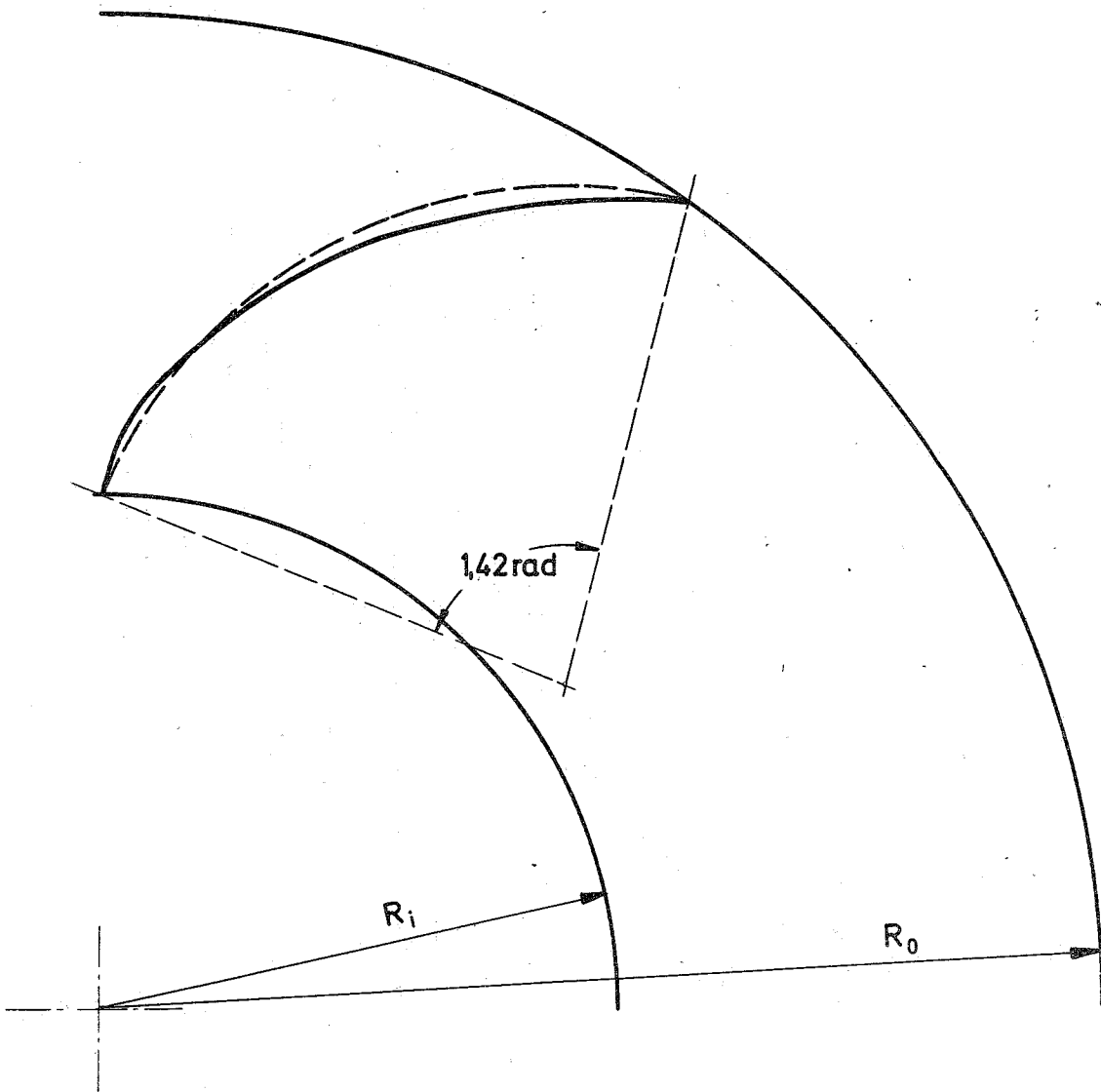
Fig.8. Transversal cross-section of the core

R_i = inner radius

R_o = outer radius

———— evolvent fuel plate

— —— circumference arc by which the evolvent is approxi-
mated in the calculation of the critical velocity